

Review

Recent Studies on the Aromaticity and Antiaromaticity of Planar Cyclooctatetraene

Tohru Nishinaga *, Takeshi Ohmae and Masahiko Iyoda

Department of Chemistry, Graduate School of Science and Engineering, Tokyo Metropolitan University, Hachioji, Tokyo 192-0397, Japan; E-Mails: ohmae-takeshi@ed.tmu.ac.jp (T.O.); iyoda@tmu.ac.jp (M.I.)

* Author to whom correspondence should be addressed; E-Mail: nishinaga-tohru@tmu.ac.jp.

Received: 29 December 2009; in revised form: 23 January 2010 / Accepted: 4 February 2010 /

Published: 5 February 2010

Abstract: Cyclooctatetraene (COT), the first $4n\pi$ -electron system to be studied, adopts an inherently nonplanar tub-shaped geometry of D_{2d} symmetry with alternating single and double bonds, and hence behaves as a nonaromatic polyene rather than an antiaromatic compound. Recently, however, considerable 8π -antiaromatic paratropicity has been shown to be generated in planar COT rings even with the bond alternated D_{4h} structure. In this review, we highlight recent theoretical and experimental studies on the antiaromaticity of hypothetical and actual planar COT. In addition, theoretically predicted triplet aromaticity and stacked aromaticity of planar COT are also briefly described.

Keywords: antiaromaticity; cyclooctatetraene; NMR chemical shifts; quantum chemical calculations; ring current

1. Introduction

Cyclooctatetraene (COT) was first prepared by Willstätter in 1911 [1,2]. At that time, the special stability of benzene was elusive and it was of interest to learn the reactivity of COT as the next higher vinyllog of benzene. However, unlike benzene, COT was found to be highly reactive to electrophiles just like other alkenes. This is because the ground state structure of COT is nonplanar tub-shaped geometry of D_{2d} symmetry with alternating single and double bonds [3-5]. The dihedral angle between

vicinal double bonds is 56° in the crystal structure [6] so that the π bonds cannot conjugate well with each other due to the absence of proper overlap between the neighboring p orbitals.

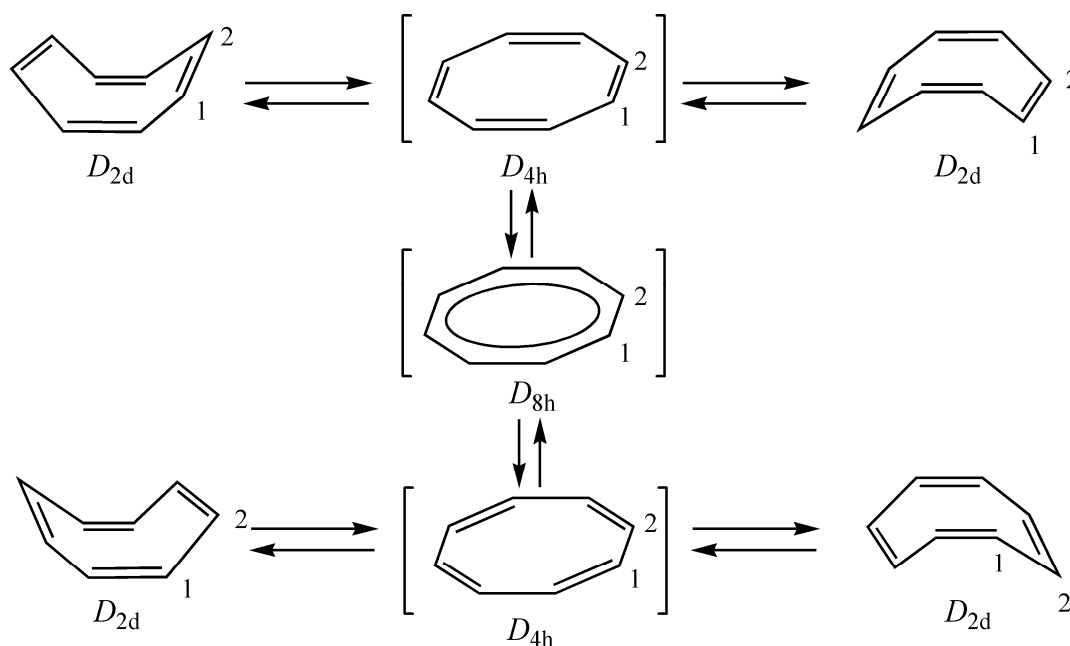
After two decades of the historical synthesis of COT, Hückel applied molecular orbital (MO) theory to monocyclic conjugated system using the π -electron approximation, and explained why cyclic delocalization of $(4n+2)$ π -electron systems causes unusual stability [7], which is now recognized as aromaticity. The theory also predicted that the highest occupied MO of cyclic π -conjugated systems with $4n\pi$ -electrons should consist of a pair of half-filled and degenerate nonbonding orbitals. Accordingly, cyclic conjugation of $4n\pi$ -electrons is considered to be energetically unfavorable. In fact, some $4n\pi$ -electron systems such as cyclobutadiene [8,9] and cyclopropenyl anion [10,11] led to strong destabilization of the compound in contrast to the stabilization characteristic of aromatic compounds. Breslow proposed the term of antiaromaticity to describe such systems [12,13].

Based on Hückel MO theory, 8π -electron system of COT with a planar and delocalized D_{8h} structure is predicted to have a triplet ground state. However, ab initio complete-active-space self-consistent-field (CASSCF) calculations showed that open-shell singlet state of COT with a D_{8h} structure is more stable than the triplet state [14]. The violation of Hund's rule was explained by the "disjoint diradicals" [15,16]. On the other hand, a planar and bond alternated D_{4h} structure should have a closed-shell singlet state where the degeneracy of the frontier orbitals for the D_{8h} structure is removed by a Jahn-Teller distortion. These singlet D_{8h} and D_{4h} structures are the presumable transition states of double bond shift and ring inversion of COT (Figure 1), although nonplanar crown- [17] and saddle-like conformations [18-21] were discussed as alternative transition state for the double bond shift. Accordingly, the barriers for both double bond shift and ring inversion should be related to the energetic aspect of antiaromaticity of COT. The inversion barrier have been measured via various methods and was found to be $10\text{--}13 \text{ kcal mol}^{-1}$ [22-25], while the barrier to bond shift was shown to be $2\text{--}4 \text{ kcal mol}^{-1}$ higher than the inversion barrier [22,23,26], even though steric effects in substituted COTs tend to increase the barrier for both bond shift and ring inversion [27, 28] and steric effects also reduce the difference between the two barriers in multiply substituted COTs [27]. Since the inner angle of the planar COT (135°) is larger than the ideal bond angle for sp^2 hybridized carbon (120°), there are some strains in the planar D_{8h} and D_{4h} transition states, and hence the antiaromatic destabilizations in both D_{8h} and D_{4h} structures are at most several kcal mol^{-1} . In accord with this explanation, the hydrogen transfer energy for the planar D_{4h} COT going to cyclooctatriene was reported to be -8 kcal mol^{-1} (B3LYP/6-311+G*) and -9 kcal mol^{-1} (MP2/6-311+G*) [9], whereas isodesmic ($27.8 \text{ kcal mol}^{-1}$ MP2/6-31G*//HF/3-21G [29]; $28.4 \text{ kcal mol}^{-1}$ MP4SDTQ/6-31G**//MP2/6-31G**+ZPE(HF/6-31G*) [30]) and homodesmic ($-28.4 \text{ kcal mol}^{-1}$ [30]) stabilization energies gave rather different results.

The other important criteria for the study of aromaticity and antiaromaticity are related to the magnetic properties of compounds. Aromatic compounds sustain diatropic ring currents with bond length equalization, while antiaromatic compounds sustain paratropic ring currents in spite of localized structures [31-34]. As a result, diatropic ring currents cause exaltations of diamagnetic susceptibility from the sum of that of acyclic reference compounds [35,36]. Also in NMR chemical shifts, shielding and deshielding effects are observed inside and outside aromatic rings, respectively, while antiaromatic paratropicity results in the opposite effects [32,34]. These phenomena can be detected experimentally. However, the comparable quantification may be difficult because the diamagnetic susceptibility

exaltations depend on the references selected and because many environmental factors affect NMR chemical shifts. On the other hand, there have been several approaches to estimate the ring current intensities using theoretical calculations. Among them, nucleus independent chemical shift (NICS) developed by Schleyer *et al.* [37,38] is one of the most used index because of the simplicity and efficiency of the methods. The methods for the visualization of ring currents such as CTOCD-DZ (continuous transformation of origin of current density - diamagnetic zero) [39,40] have also been developed recently. By using these methods, studies on the antiaromatic paratropicity of planar COTs have progressed. In this review, we highlight recent theoretical and experimental studies on the antiaromaticity based on the magnetic properties of hypothetical planar COT and related planarized COT annelated with ring units [41]. In addition, theoretically predicted triplet aromaticity and stacked aromaticity of planar COT are also briefly described.

Figure 1. Schematic drawings of ring inversion and double bond shift of D_{2d} COT via D_{4h} and D_{8h} transition states, respectively.



2. Unsubstituted COT

Since planar conformations of unsubstituted COT are considered to be the transition states of ring inversion and bond shift, it is difficult to experimentally investigate the planar COT [25] and most studies have been performed with quantum chemical calculations. In this section, computational studies of the aromaticity and antiaromaticity of planar COT based on NICS and CTOCD-DZ are summarized.

2.1. Computational Studies Based on NICS

The degrees of aromaticity of tub-shaped D_{2d} (singlet (S_0)) and planar D_{4h} (S_0) and D_{8h} (open-shell S_0 and triplet (T_1) states) COT that have been assessed using NICS criteria are summarized in Table 1,

together with the bond lengths of each optimized geometries [38,42,43]. The NICS(0) value of tub-shaped D_{2d} COT is +3.0 at the GIAO/HF/6-31+G* level using the B3LYP/6-311+G** optimized geometry [42]. The small value is in line with the expected nonaromatic character due to the bent structure. On the other hand, effect of bending of the C=C–H angle directed toward the double bond in D_{2d} COT was investigated [44]. The bending of the C=C–H angle causes increase of NICS value with increasing planarity of the COT ring and decreasing HOMO–LUMO gap.

Table 1. C–C Bond lengths and NICS(0) values for the S_0 and T_1 states of COT.

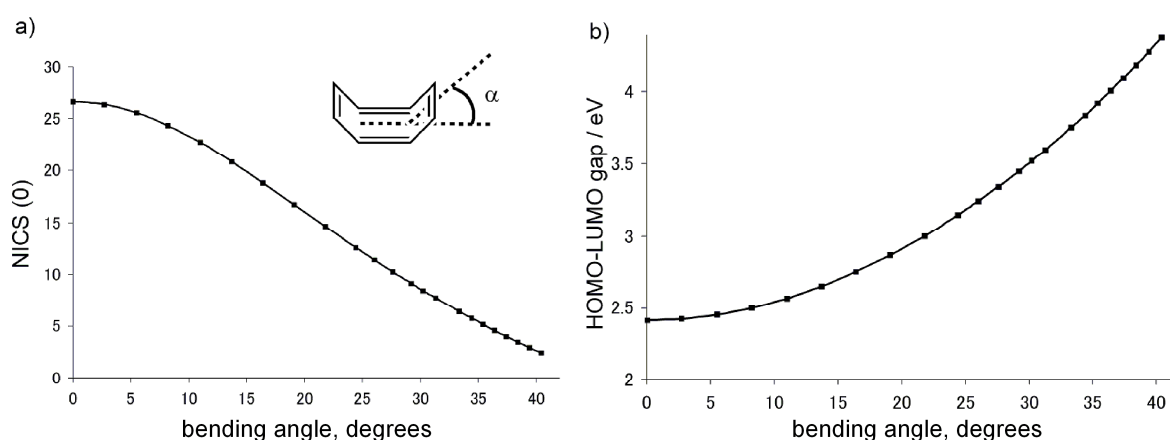
molecule	state	method (geometry)	C–C bond length (Å)	method (magnetic properties)	NICS(0) (ppm)	ref.
C ₈ H ₈ (D_{2d})	S_0	B3LYP/6-311+G**	1.340 1.472	GIAO/HF/6-31+G*	+3.0	[42]
		HF/6-31G**	1.344 1.479	GIAO/HF/6-311+G*	+1.9	[43]
				GIAO/CASSCF(8,8) /6-311+G*	+1.2	[43]
C ₈ H ₈ (D_{4h})	S_0	B3LYP/6-31G*	N.R.	GIAO/HF/6-31+G*	+30.1	[38]
		HF/6-31G**	1.351 1.472	GIAO/HF/6-311+G*	+29.3	[43]
				GIAO/CASSCF(8,8) /6-311+G*	+16.1	[43]
C ₈ H ₈ (D_{8h})	S_0	CASSCF(8,8) /6-31G**	1.408	GIAO/CASSCF(8,8) /6-311+G*	+40.7	[43]
		B3LYP/6-311+G**	1.403	GIAO/HF/6-31+G*	–12.4	[42]
	T_1	CASSCF(8,8) /6-31G**	1.406	GIAO/HF/6-311+G*	–12.1	[43]
				GIAO/CASSCF(8,8) /6-311+G*	–8.9	[43]

In addition, to investigate the relationships among the strength of paratropicity, the HOMO–LUMO gap, and the bent angle α of the COT ring, the NICS values and the HOMO–LUMO gaps of COT with various bent angles were calculated at the GIAO/HF/6-311+G**//B3LYP/6-31G** level [45] and the results are plotted in Figure 2. As the bent angle decreases, the NICS value of the COT ring increases (Figures 2a), with considerable narrowing of the HOMO–LUMO gap (Figure 2b).

The NICS(0) value of planar COT with bond alternated D_{4h} symmetry was reported in the first paper of NICS [38]. The value is +30.1 at the GIAO/HF/6-31+G* level using the B3LYP/6-31G* optimized geometry, suggesting that the considerable antiaromatic paratropicity is generated in the planar COT ring even with the bond alternated structure. Similar result (+29.3) was obtained for D_{4h} COT at the GIAO/HF/6-311+G**//HF/6-31G** level [43]. However, the NICS(0) value was shown to be considerably reduced when the CASSCF-GIAO method was used. The value (+16.1) of D_{4h} COT at

the CASSCF-GIAO level is almost half of that of HF-GIAO method. It is also much smaller than that (+40.7) of D_{8h} COT at open-shell S_0 state by factor of 2.3 [43]. For the estimation of NICS value of D_{8h} COT at S_0 state, the use of CASSCF-GIAO is essential, and hence such a large discrepancy is only observed in the method. In any case, the NICS-based studies showed that the antiaromatic paratropicity of planar COT is highest for the D_{8h} structure at open-shell S_0 state and considerable antiaromaticity is retained for D_{4h} structure despite of the small barriers for ring inversion and bond shift of COT ring.

Figure 2. Correlations between a) NICS(0) (GIAO/HF/6-311+G**//B3LYP/6-31G**) and bent angle α and b) HOMO–LUMO gap (B3LYP/6-31G**) and bent angle α of cyclooctatetraene.



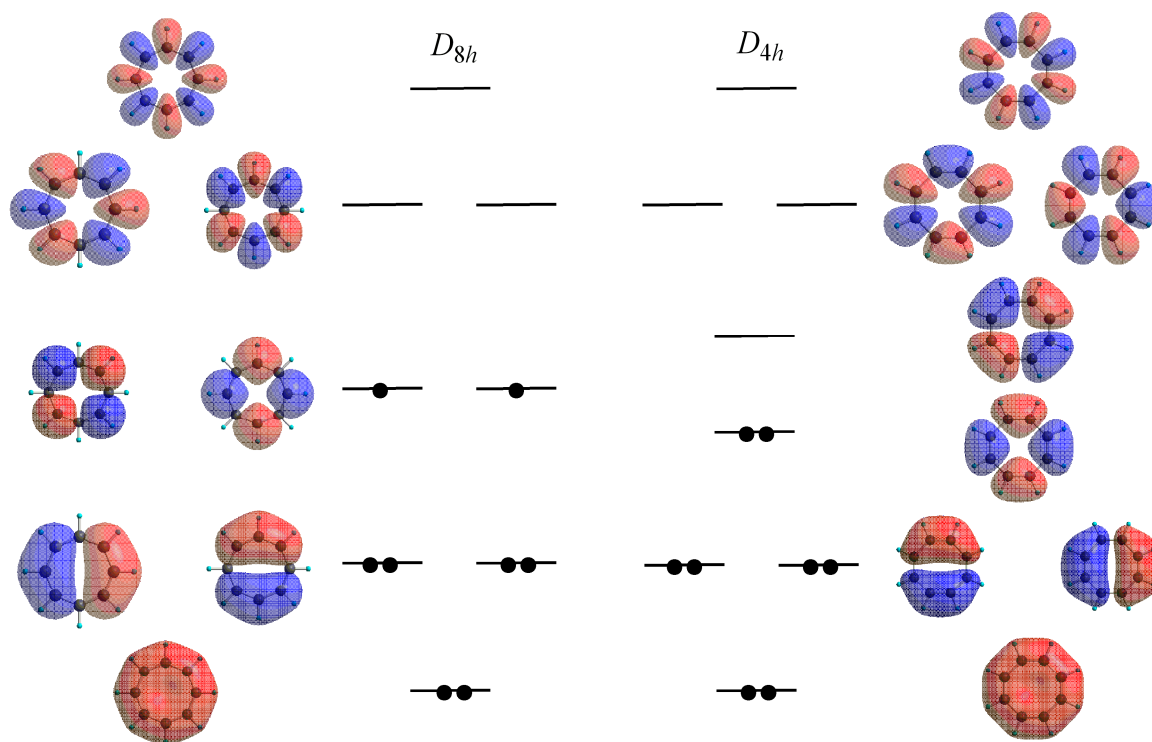
As concerns the lowest T_1 state of D_{8h} COT, not antiaromaticity but rather aromaticity is expected. The idea that triplet $4n\pi$ -electron annulene is regarded as being aromatic was originally suggested in 1972 [46] using its Dewar resonance energy. Other studies supported the aromaticity of $4n\pi$ -electron annulene [47,48]. The NICS calculations also supported the aromaticity of D_{8h} COT at T_1 state. The NICS(0) value is -12.4 at the GIAO/HF/6-31+G**//B3LYP/6-311+G** [42], which is, however, more negative than that (-8.9) of CASSCF-GIAO method [43]. Another study based on scanning NICS over a distance and separating them into in-plane and out-of plane contributions also confirmed the aromaticity of D_{8h} COT at T_1 state [49]. It is to be noted that the C–C bond lengths of D_{8h} COT at both S_0 and T_1 states are almost identical irrespective of the antiaromatic and aromatic characters, respectively [43].

2.2. Computational Studies Based on CTOCD-DZ

In CTOCD-DZ, a point, at which the induced current density is calculated, is taken as the origin of vector potential and the accumulated vectors yield three-dimensional induced molecular current distributions. In addition, the current maps can be expressed as sums of the possible orbital contributions. By taking advantage of the latter feature, orbital contribution in the paratropic ring current of D_{4h} COT was investigated [50,51]. As mentioned above, D_{8h} COT has a pair of half-filled and degenerate nonbonding orbitals, while the degeneracy is removed by a Jahn-Teller distortion in D_{4h} COT (Figure 3). As a result, the HOMO–LUMO pair split into two non-degenerate components

with a narrow HOMO–LUMO gap. This causes a rotational transition with a small energy and thereby produces a strong paramagnetic ring current. CTOCD-DZ clearly demonstrated that the paratropic ring current in D_{4h} COT is dominated by the HOMO–LUMO transition [50,51], meaning the paratropicity corresponds to circulation of only two-electrons in the frontier orbitals.

Figure 3. π -Molecular orbitals and their orbital energy schemes for D_{8h} and D_{4h} COT.



Furthermore, the paratropic ring currents in tub-shaped D_{2d} COT were also investigated by means of CTOCD-DZ [52]. In the study, d (Å) value is defined as the distance between the planes of the upper and bottom four carbons of tub-shaped COT ring. The paratropic ring current was shown to survive even in a tub-shaped COT ring when d is below 0.62 Å. Since d of the equilibrium structure of tub-shaped COT is 0.76 Å, the paratropic current survive until 80% of the geometric change.

3. COTs Planarized by Annellation

3.1. Attempted syntheses

In the initial synthetic study to realize planar [8]annulene, triple bonds were introduced and dibenzocyclooctadiene-3,7-diyne (**1**) and dibenzocyclooctatriene-7-yne (**2**) (Figure 4) were prepared [53–55]. X-ray studies of diyne **1** demonstrated that the [8]annulene core has a planar structure [56]. However, the antiaromatic paratropicity of **1** as well as **2** is considerably attenuated judging from the NICS(0) value of **1** (+4.04 at the GIAO/B3LYP/6-31G* level) [57].

For the other methods without using triple bond, there are two strategies to constrain the inherently non-planar COT ring to adopt a planarized conformation. They are the annellation of either small membered rings or rigid planar π -systems to the COT skeleton. In the former structural modification,

the annelated small ring causes widening of the exocyclic bond angle which corresponds to the inner angle of the COT ring. Since the average inner angle of octagon (135°) is larger than the ideal bond angle for sp^2 hybridized carbon (120°), the widening of the inner angle of COT ring brings about some planarization. By the use of this method, COTs **3-5** annelated with one three- or four-membered ring (Figure 5) have been prepared.

Figure 4. Chemical structure of dibenzocyclooctadiene-3,7-diyne (**1**) and dibenzocyclooctatriene-7-yne (**2**).

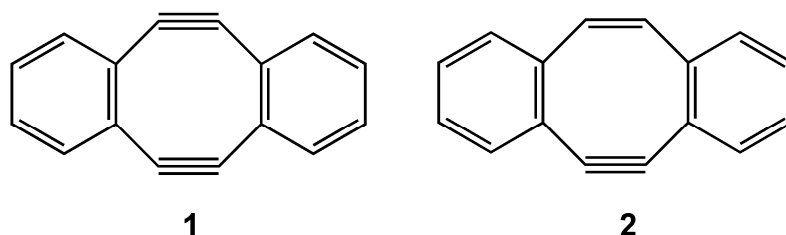
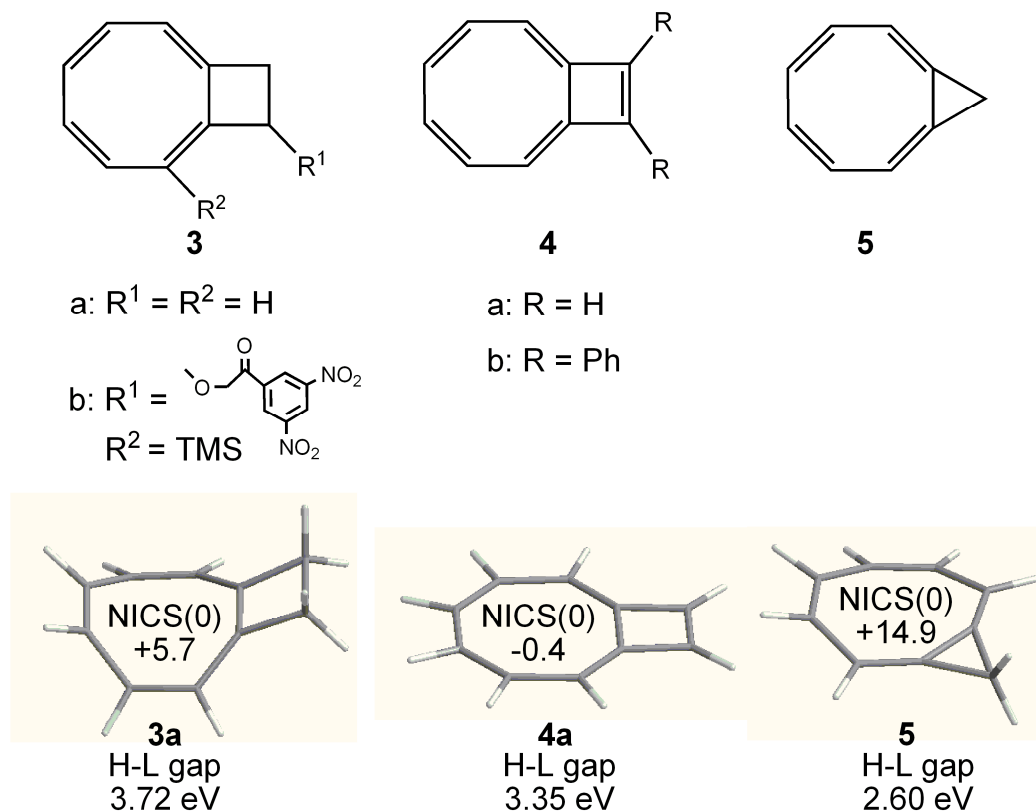


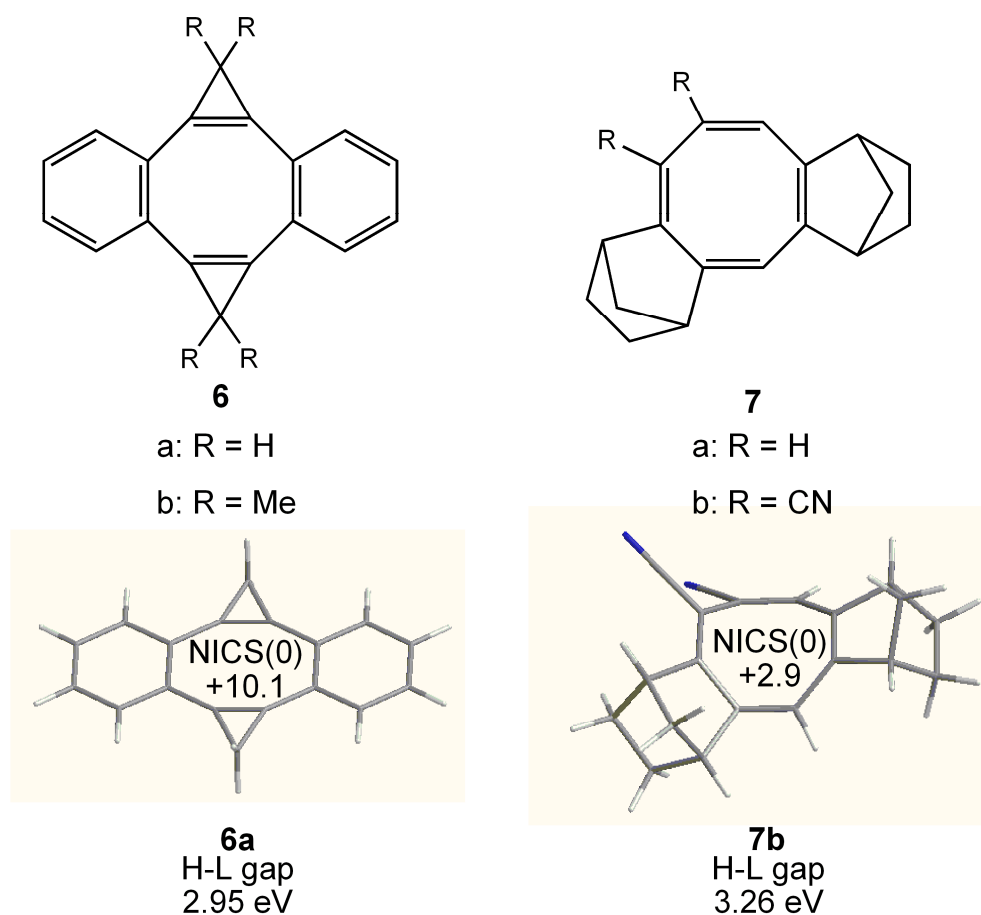
Figure 5. Chemical structure of cyclobuteno-COT **3**, bicyclo[6.2.0]decapentaene **4** and cycloprop[8]annulene **5**. Calculated geometry, NICS(0) (GIAO/HF/6-311+G**//B3LYP/6-31G**) and HOMO–LUMO (H-L) gap (B3LYP/6-31G**) of **3a**, **4a**, and **5** are also shown.



Among them, the parent **3a** readily polymerizes when concentrated [58,59] and substituted derivative **3b** is the first example that the X-ray structure of cyclobuteno-COT has been determined [60]. However, the effect of planarization by the annelation of cyclobutene ring is quite small as

predicted by the molecular mechanics calculations [61]. One additional double bond to **3** was shown to be quite effective for planarization of the eight-membered ring and bicyclo[6.2.0]decapentaene **4a** [62] and its diphenyl derivative **4b** [63] were shown to have a nearly planar conformation. However, the X-ray structural analysis [63] suggested that **4** is not 8π -antiaromatic COT but rather a 10π -aromatic system like azulene. CTOCD-DZ calculations supported the conclusion [64]. Cycloprop[8]annulene **5** has a planarized tub-conformation, and some paratropic ring current was found to be induced as ^1H NMR chemical shifts of the protons in the eight-membered ring appears at δ 3.6–3.7 ppm which is ca. 2 ppm upfield shifted from that of parent COT (δ 5.68) [65]. CTOCD-DZ calculations supported the presence of a paratropic ring current in **5** [52]. Here, we also calculated NICS(0) value (GIAO/HF/6-311+G**//B3LYP/6-31G**) and HOMO–LUMO gap (B3LYP/6-31G**) of **3a**, **4a**, and **5** (Figure 5), and only **5** showed a relatively large positive NICS value in accord with the observed large upfield shift of the ring protons.

Figure 6. Chemical structure of bis-cyclopropeno-COT **6** and bis-norborneno-COT **7**. Calculated geometry, NICS (0) (GIAO/HF/6-311+G**//B3LYP/6-31G**) and HOMO–LUMO (H–L) gap (B3LYP/6-31G**) of **6a** and **7b** are also shown.

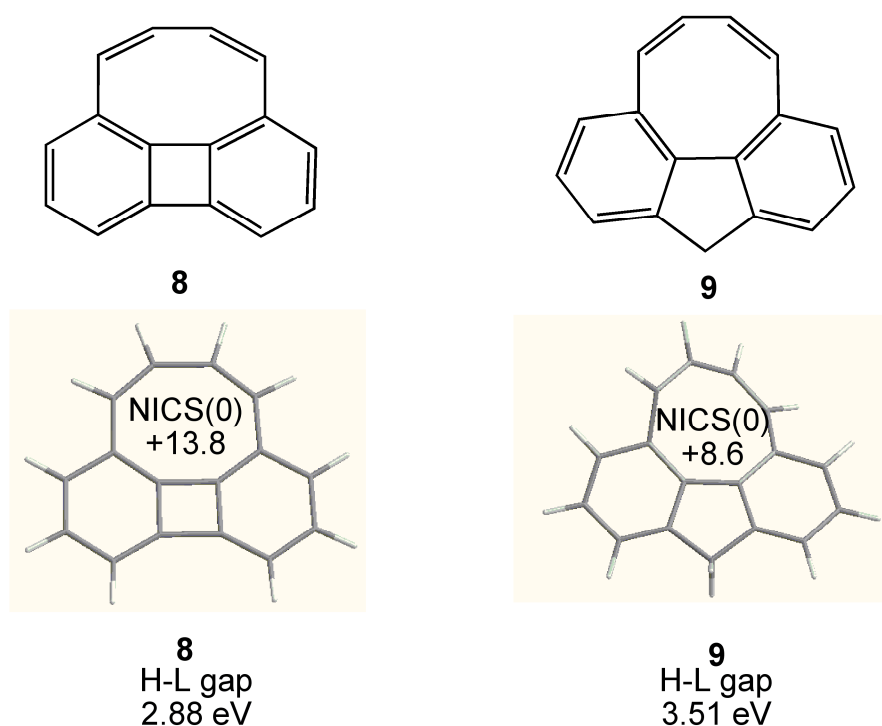


COTs **6** and **7** annelated with two cyclopropene ring or norbornene units (Figure 6) have also been prepared. Concerning about **6**, a planar [8]annulene core was demonstrated in **6b** [66], but the NICS(0) value of **6a** (+10.1) is considerably reduced due to the deformed eight-membered ring and/or the annelation of benzene rings. As for **7a**, the author predicted that the COT ring could be planarized by

the annelation with the rigid small rings at C1, C2 and C4, C5 position [67]. However, the X-ray structure of **7b** revealed that the COT ring is not planar [68] and NICS(0) value of **7b** (+2.9) is as small as that of D_{2d} COT at the ground state.

As the second strategy for the planarization of COT ring, the annelation of rigid planar π -systems to COT ring has also been investigated. The first example is COT annelated with biphenylene **8** [69,70]. As shown in Figure 7, the COT ring is almost planar but considerably deformed. Thus, although some upfield shift in ^1H NMR of the olefinic protons (δ 4.62) was observed in comparison with those of nonplanar biphenyl analogue (δ 6.82, 6.32) [71], the antiaromatic paratropicity is not so large judging from the NICS(0) value. The reduced antiaromaticity may be caused by the deformed eight-membered ring and/or the annelation of aromatic two benzene units. Similarly, COT annelated with fluorene **9** [71] was prepared and some upfield shift in ^1H NMR of the olefinic protons (δ 5.90, 5.68) was also observed. However, the antiaromatic paratropicity is small due to the non planar COT ring.

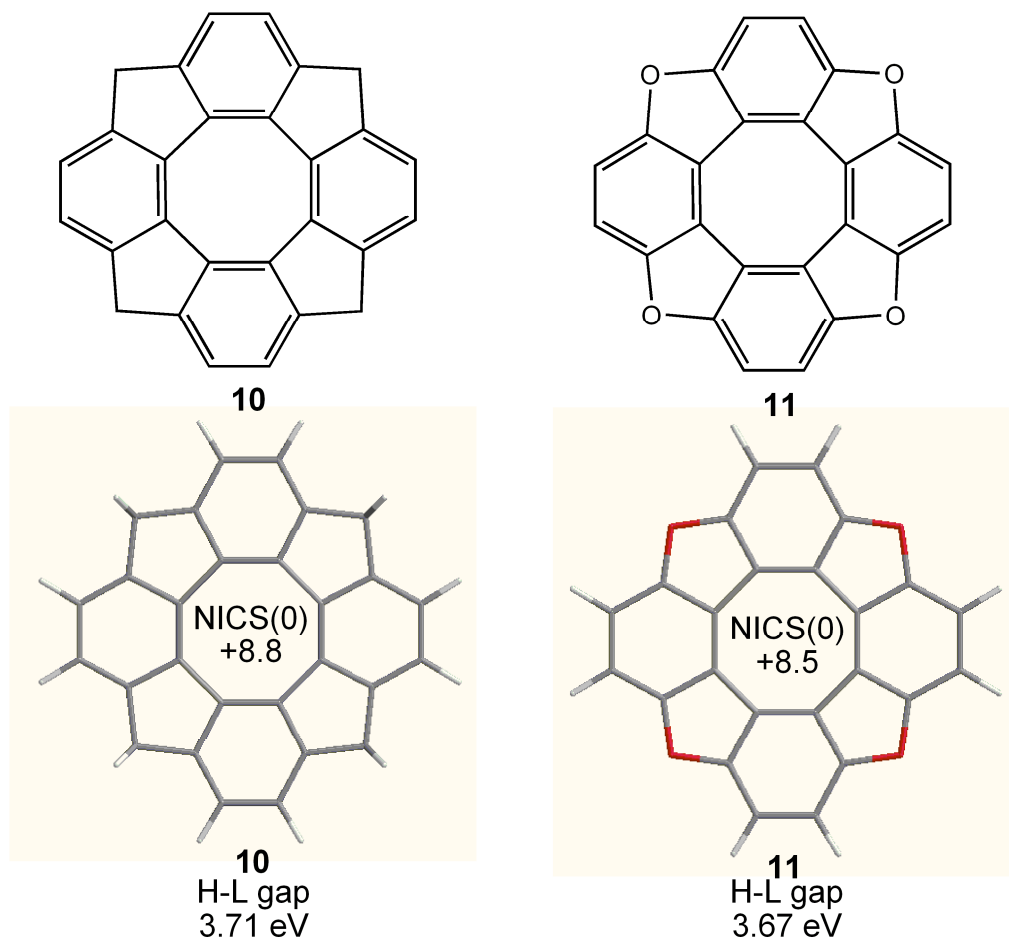
Figure 7. Chemical structure of cycloocta[*def*]biphenylene **8** and cycloocta[*def*]fluorene **9**. Calculated geometry, NICS(0) (GIAO/HF/6-311+G**//B3LYP/6-31G**) and HOMO–LUMO (H–L) gap (B3LYP/6-31G**) of **8** and **9** are also shown.



On the other hand, the tetraphenylene completely planarized by four methylene and oxygen bridges **10** [72] and **11** [73] (Figure 8) have a higher D_{4h} symmetry. However, both NICS(0) values exhibit smaller antiaromatic character in the central eight-membered ring than that of **8**, suggesting that the paratropicity of the COT ring is weakened by the annelation of aromatic benzene rings [45].

Thus, the design of complete planarization of the COT ring with substantial paratropicity has been rather difficult and only several types of derivatives have so far been known as summarized below.

Figure 8. Chemical structure of bridged tetraphenylenes **10** and **11**. Calculated geometry, NICS(0) (GIAO/HF/6-311+G**//B3LYP/6-31G**) and HOMO–LUMO (H-L) gap (B3LYP/6-31G**) of **10** and **11** are also shown.



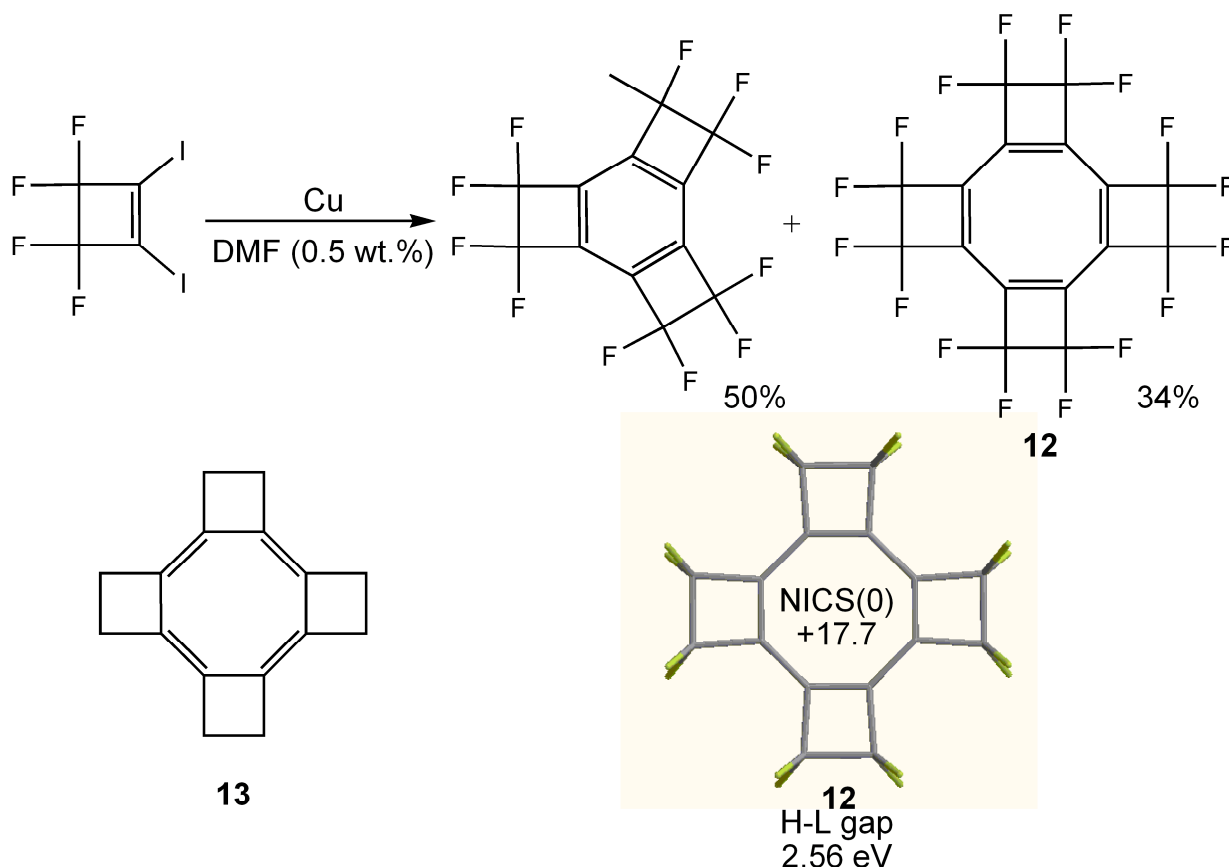
3.2. Planar COT Annelated with Four Cyclobutene Rings

Planar COT **12** tetra-annelated with tetrafluorocyclobutene units has been synthesized by copper-mediated coupling reaction of 3,3,4,4-tetrafluoro-1,2-diiodo-1-cyclobutene in the presence of 0.5 wt.% of DMF (Figure 9) [74]. X-ray crystallography of **12** demonstrated the planar and bond-alternated COT structure with the shorter bonds endocyclic to the cyclobutene rings [75] and the structural features were reproduced by theoretical calculations [76,77]. The position of the double bonds in **12** is in contrast to the structure of hypothetical hydrocarbon analogue **13** in which the shorter bonds are theoretically predicted to be exocyclic to the cyclobutane rings [76].

The color of **12** is deep red, suggesting that **12** has a relatively narrow HOMO–LUMO gap and hence a strong paratropic ring current. In fact, CTOCD-DZ calculations predicted that **12** as well as **13** have a strong paratropic ring current [78]. We also calculated the HOMO–LUMO gap (B3LYP/6-31G**) and NICS(0) value (GIAO/HF/6-311+G**) and the results were 2.56 eV and +17.7 ppm. These values are narrower and larger than those of **3-11**. It is interesting to note that **12** has an extraordinarily low reduction potential (+0.79 V vs SCE; +0.33 V vs Fc/Fc⁺) owing to lowering of the

LUMO level by planarization of COT ring and the accumulated electron-withdrawing effects of sixteen fluorine atoms [79].

Figure 9. Synthetic scheme for **12** and chemical structure of **13**. Calculated geometry, NICS(0) (GIAO/HF/6-311+G**//B3LYP/6-31G**) and HOMO–LUMO (H-L) gap (B3LYP/6-31G**) of **12** are also shown.

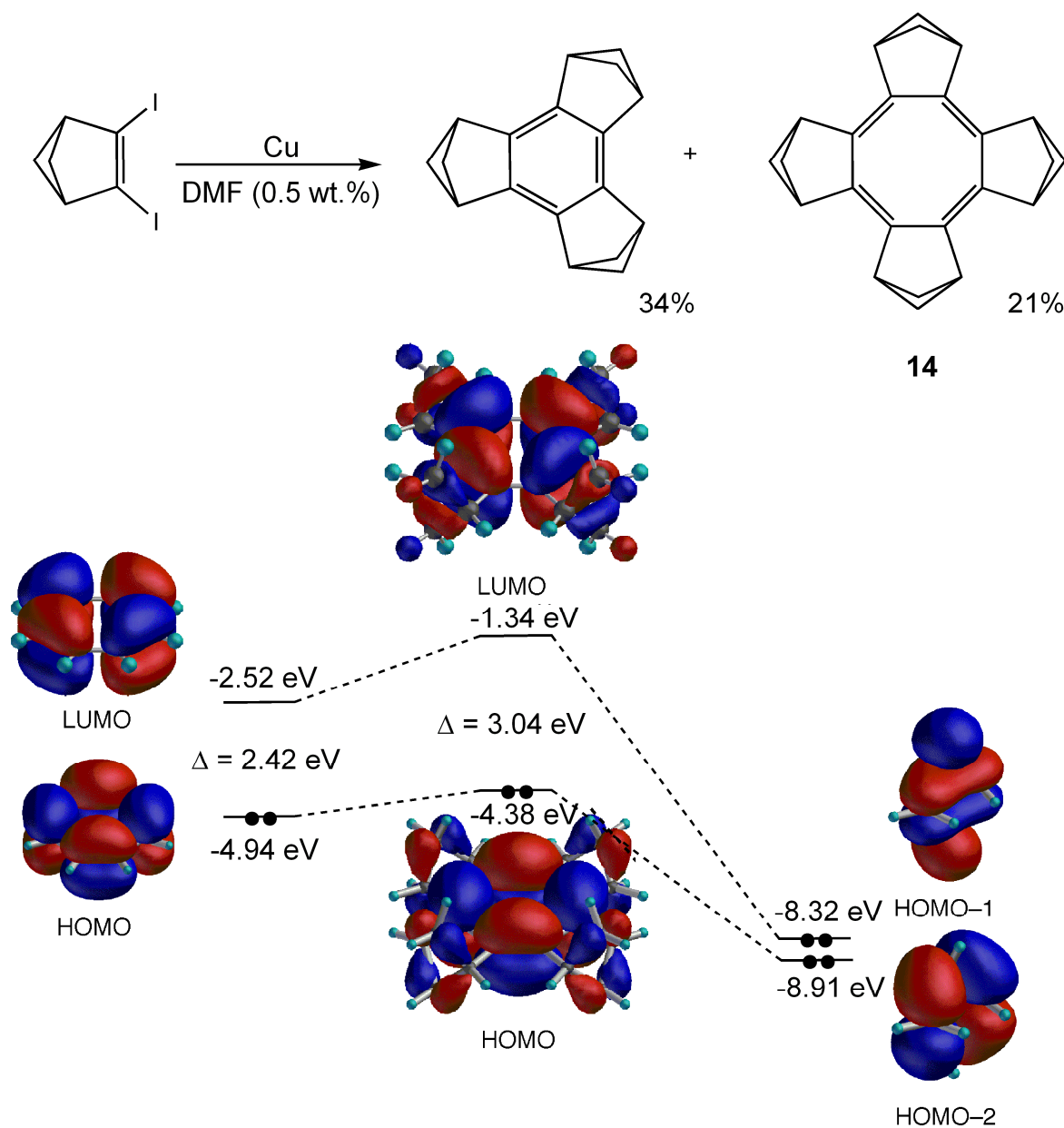


3.3. Planar COT Annelated with Plural Bicyclo[2.1.1]hexene Rings

Planar COT **14** tetra-annellated with bicyclo[2.1.1]hexene units has been synthesized by copper-mediated coupling reaction of 1,2-diodobicyclo[2.1.1]hex-2-ene (Figure 10) [80]. X-ray crystallography of **14** demonstrated the planar and bond-alternated COT structure with the shorter bonds exocyclic to the cyclobutene rings as predicted by the theoretical calculations [76]. The bond-alternation in **14** ($\Delta R_{\text{obs}} = R_{\text{endo}} - R_{\text{exo}} = 1.500(1) - 1.331(1) = 0.169 \text{ \AA}$) is much larger than that of **12** (obs: $R_{\text{endo}} = 1.353(10)$, $R_{\text{exo}} = 1.425(14)$ [75]; $\Delta R_{\text{calc}} = R_{\text{exo}} - R_{\text{endo}} = 1.454 - 1.359 = 0.095 \text{ \AA}$ (B3LYP/6-31G**)), which would be caused by the annelation with highly strained bicyclo[2.1.1]hexene units. The color of **14** is red with weak absorption band at 459 nm ($\log \epsilon = 2.11$), indicating a relatively narrow HOMO–LUMO gap for an 8π -electron system. However, the NICS value of **14** (+10.6) at the GIAO/HF/6-31+G**//B3LYP/6-31G* level [80] is considerably reduced in comparison with that of D_{4h} COT (+27.2) at the same level, although CTOCD-DZ calculations support that **14** sustains a weak paratropic ring current [78]. The large bond alternation in **14** is not the main reason for the considerable decrease in antiaromatic paratropicity, since a much larger NICS value

(+22.1) was calculated for a hypothetical planar COT having exactly the same bond lengths as those in **14** [81]. As described in section 2.2, the HOMO–LUMO transition dominates the total π ring current in planar COT and determines its paratropic nature [50]. Thus, the relatively larger HOMO–LUMO gap (3.04 eV at the B3LYP/6-31G* level) for a planar COT, in which the LUMO level is raised by the orbital interaction with the annelated bicyclic ring (Figure 10), is considered to be the main reason for the reduced antiaromaticity in **14**.

Figure 10. Synthetic scheme for **14** and the HOMO and LUMO calculated at the B3LYP/6-31G(d) level for **14** and for D_{4h} COT together with orbital interaction diagrams between the COT and puckered cyclobutane rings of bicyclo[2.1.1]hexene units.

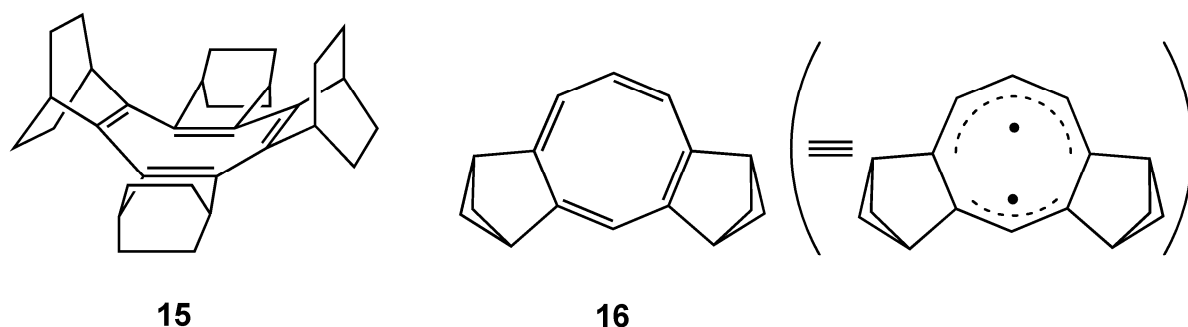


Planar COT **14** has an unusually low oxidation potential (+0.07 V vs Fc/Fc^+) and gives a fairly stable radical-cation salt [82]. This is ascribed to the raised HOMO level due to the σ – π conjugative effects of bicyclic frameworks in addition to a narrowed HOMO–LUMO gap by the planarization of

COT ring as shown in Figure 10. Interestingly, the longest wavelength absorption (630 nm) of radical cation of planar **14** is blue-shifted from that (745nm) of radical cation of tub-shaped COT fully annelated with bicyclo[2.2.2]octene units **15** (Figure 11) [83], indicating the planarization causes hypsochromic shift contrary to the common sense for effective π -conjugations. This is due to the widening of the HOMO–SOMO gap caused by the raised SOMO (HOMO in neutral COT) and lowered HOMO (HOMO⁻¹ in neutral COT) accompanying the flattening of the COT ring. The lower HOMO⁻¹ level of planar neutral COT may be the principal contributor to the small antiaromatic destabilization for COT ring (See Introduction).

Another COT annelated with two bicyclo[2.1.1]hexene units **16** (Figure 11) has also been theoretically predicted to have a planar structure [76]. In this compound, singlet diradicaloid state is the minimum energy form just like open-shell singlet state of COT with a D_{8h} structure [14].

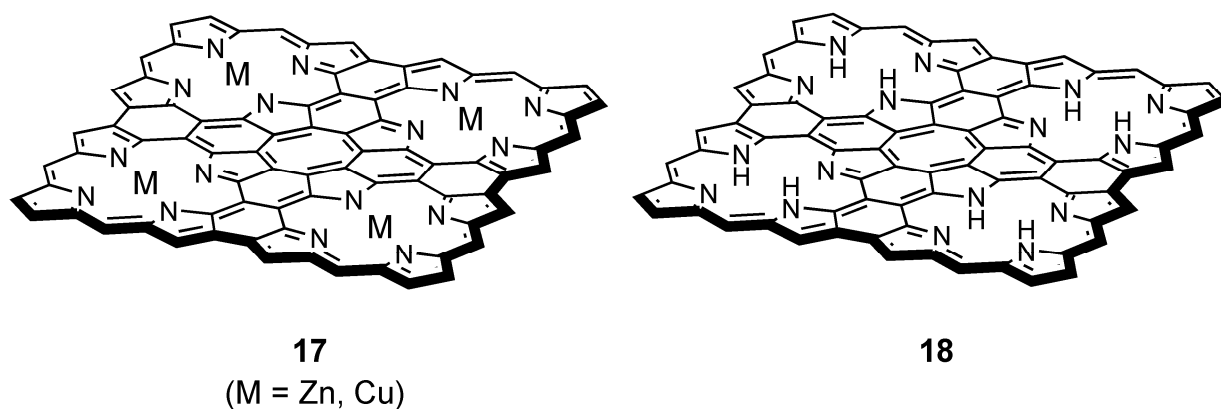
Figure 11. Chemical structure of COTs fully annelated with bicyclo[2.2.2]octene units **15** and annelated with two bicyclo[2.1.1]hexene units **16**.



3.4. Planar COT Annelated with Porphyrin Rings

Directly fused tetrameric porphyrin sheets **17** and their free base analogue **18** (Figure 12), which are also calculated to have a planar COT core, have been synthesized [84,85]. The directly meso-meso linked cyclic porphyrin tetramer which is the precursor for **17**(Zn), was synthesized through a stepwise coupling reaction sequence. Then the precursor was treated with 30 equiv of DDQ and Sc(OTf)₃ to give **17**(Zn) as black solid. Free base sheet **18** was obtained by demetallation of **17** [85]. As for the paratropicity of the central COT ring, NICS calculations were performed at the GIAO/B3LYP/6-31G*//B3LYP/6-31G* level (LANL2DZ for zinc atom) and the values were +61.7 for **17**(Zn) and +21.7 for **18** (29.2 for D_{4h} COT at the same level) [84]. The distance-dependent NICS at the center of the COT core for **17**(Zn) was also performed [86], which was shown to decrease monotonously with increasing distance as shown in the case of cyclobutadiene [87]. Furthermore, the complex of **17**(Zn) with 1,4-bis(1-methylimidazol-2-ylethynyl)benzene or 5,15-bis(1-methylimidazol-2-yl)-10,20-dihexylporphyrin experimentally proved the paratropic ring current of the central COT core [84]. However, in spite of the large difference between the NICS values of **17**(Zn) and **18**, the absorption spectra of **17** and **18** is quite similar [85], suggesting that the HOMO–LUMO gaps of **17** and **18** are almost identical.

Figure 12. Chemical structure of directly fused tetrameric porphyrin sheets **17** and its free base analogue **18**.

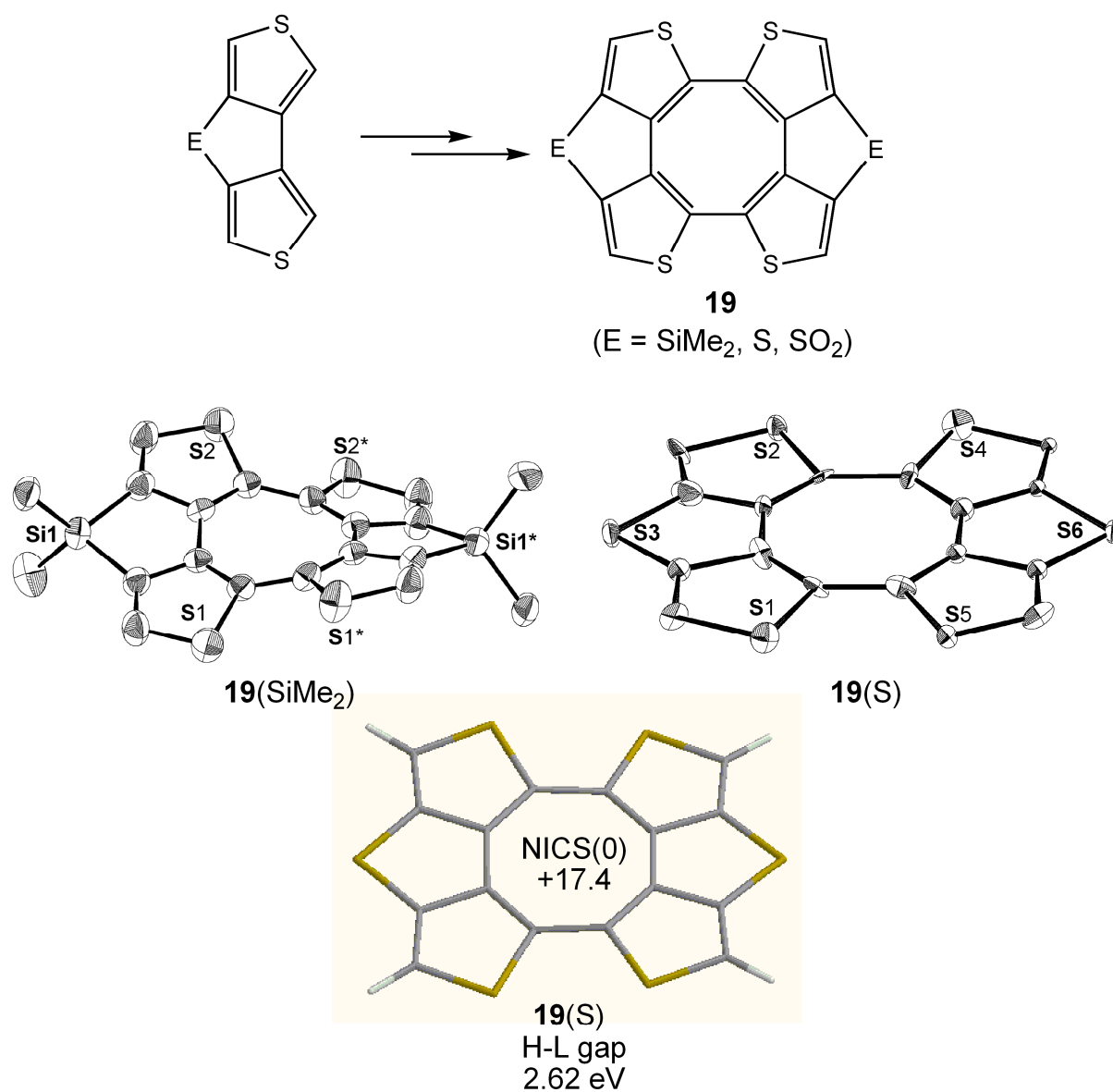


3.5. Planar COT Annelated with Thiophene Rings.

Cyclic tetrathiophenes **19** planarized by dimethylsilyl, sulfur, and sulfone bridges bearing a planarized COT core (Figure 13) have been synthesized by homocoupling of the bridged bithiophene precursors [45]. The bent angle of the central COT rings of **19** can be finely adjusted by using the small differences in the bond lengths between the bridging units and thiophene rings and the planarity is enhanced in the order of **19(S)** > **19(SO₂)** > **19(SiMe₂)** (See X-ray structures of **19(S)** and **19(SiMe₂)** in Figure 13). From the comparisons of NICS values (**19(S)**: +17.4; **19(SO₂)**: +15.4; **19(SiMe₂)**: +12.7 (GIAO/HF/6-311+G**//B3LYP/6-31G**)) and calculated HOMO–LUMO gaps (**19(S)**: 2.62 eV; **19(SO₂)**: 2.72 eV; **19(SiMe₂)**: 2.87 eV) of the optimized structures of **19**, similar enhancement of the paratropicity and narrowing of the HOMO–LUMO gap with decreasing bent angle of the COT rings as shown in Figure 2 were also demonstrated for **19**. It is interesting to note that the NICS value of **19(S)** with highest planarity among **19** is larger than those of **3–11** and almost identical to that of **12**.

The theoretically predicted relationships among the paratropicity, HOMO–LUMO gap, and planarity of the COT ring shown in Figure 2 were also qualitatively proved by means of ¹H NMR and UV-vis measurements of **19**. In comparison of the ¹H NMR chemical shifts of **19** with those of the corresponding precursors, upfield shifts due to a paratropic ring current in the COT ring were observed and the degree of shift increased with increasing planarity of the COT ring. Furthermore the absorption maxima of **19** showed bathochromic shifts with increasing planarity of the COT ring.

Figure 13. Synthetic scheme for **19** and X-ray structures of **19(S)** and **19(SiMe₂)**. Calculated geometry, NICS(0) (GIAO/HF/6-311+G**//B3LYP/6-31G**) and HOMO–LUMO (H-L) gap (B3LYP/6-31G**) of **19(S)** are also shown.

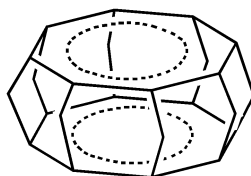


4. Stacking of Planar COT Rings

Recently, it has been shown using NICS calculations that stacking of antiaromatic annulene rings into superphane structure can reverse antiaromaticity and result in through-space three-dimensional aromatic character [88]. As for the COT ring system **20** (Figure 14), D_{8h} structure is minimum, indicating that the stacked ring aromaticity causes the bond length equalization. The NICS(0) values of the COT ring (−22.0 at the PW91/IGLOIII//B3LYP/6-311+G**) and superphane center of symmetry (−35.5) predicts the strong diatropicity of the system. From these results as well as the results for other ring size, the authors concluded that “stacking, along with triplet [42] and Möbius strategies [89,90], is the third way to render $4n\pi$ electron system aromatic.” CTOCD-DZ calculations [91] supported the

conclusion, whereas an analysis based on energetic criteria using graph theory concluded that the stacking of antiaromatic ring does not bring about aromatic stabilization energy even though the original antiaromaticity is reduced [92].

Figure 14. Chemical structure of COT superphane **20**.



20

5. Conclusions

Recent studies on aromaticity and antiaromaticity of planar unsubstituted COT based on NICS and CTOCD-DZ calculations have been summarized in section 2. These studies have revealed the paratropicity of D_{4h} and open-shell singlet D_{8h} COTs and diatropicity of triplet D_{8h} COT. Among these types of COTs, synthetically accessible derivatives have so far been limited to bond-alternated D_{4h} type structure, and the antiaromaticity of COTs planarized by annelation with various rigid rings has been assessed by NICS values. For the most classical planarized COTs, however, complete planarization of the ring with substantial paratropicity was not attained, and only a few compounds showed that the NICS(0) value is comparable to or exceeds two-third (+17.7 at the GIAO/HF/6-311+G**//B3LYP/6-31G** level) of that of D_{4h} COT (+26.6). Among them, we have attained a planar COT structure in **19(S)** without bulky substituents unlike the other planar COTs, and X-ray crystallography showed a stacking structure [45]. Thus, the structure of **19(S)** may be utilized for study on an intermolecular antiaromatic-antiaromatic interaction [88] by controlling the stacking manner with additional substituents at the side positions. Such experiments may also lead to these compounds becoming unique candidates for efficient organic electronic devices, in which the use of antiaromatic ring has not been tested.

Acknowledgements

This work was supported by Grant-in-Aid for Scientific Research on Priority Areas (No. 20036042, Synergy of Elements) and on Innovative Areas (No. 21108519, " π -Space") from the Ministry of Education, Culture, Sports, Science, and Technology of Japan.

References

1. Willstätter, R.; Waser, E. Über Cyclo-octatetraen. *Chem. Ber.* **1911**, *44*, 3423–3445.
2. Willstätter, R.; Heidelberger, M. Zur Kenntnis des Cyclo-octatetraens. *Chem. Ber.* **1913**, *46*, 517–527.
3. Karle, I.L. An Electron Diffraction Investigation of Cyclooctatetraene and Benzene. *J. Chem. Phys.* **1952**, *20*, 65–70.

4. Bastiansen, O.; Hedberg, L.; Hedberg, K. Reinvestigation of the Molecular Structure of 1,3,5,7-Cyclooctatetraene by Electron Diffraction. *J. Chem. Phys.* **1957**, *27*, 1311–1317.
5. Traetteberg, M. The Molecular Structure of 1,3,5,7-Cyclo-octatetraene. *Acta Chem. Scand.* **1966**, *20*, 1724–1726.
6. Bordner, J.; Parker, R.G.; Stanford, R.H. The Crystal Structure of Octamethylcyclooctatetraene. *Acta Crystallogr. Sect. B* **1972**, *28*, 1069–1075.
7. Hückel, E. Quantentheoretische Beiträge zum Benzolproblem. *Z. Phys.* **1931**, *70*, 204–286.
8. Bally, T. Cyclobutadiene: The Antiaromatic Paradigm? *Angew. Chem. Int. Ed.* **2006**, *45*, 6616–6619.
9. Wiberg, K.B. Antiaromaticity in Monocyclic Conjugated Carbon Rings. *Chem. Rev.* **2001**, *101*, 1317–1331.
10. Allen, A.D.; Tidwell, T.T. Antiaromaticity in Open-Shell Cyclopropenyl to Cycloheptatrienyl Cations, Anions, Free Radicals, and Radical Ions. *Chem. Rev.* **2001**, *101*, 1333–1348.
11. Breslow, R.; Brown, J.; Gajewski, J.J. Antiaromaticity of Cyclopropenyl Anions. *J. Am. Chem. Soc.* **1967**, *89*, 4383–4390.
12. Breslow, R. Antiaromaticity. *Acc. Chem. Res.* **1973**, *6*, 393–398.
13. Breslow, R. Small Antiaromatic Rings. *Angew. Chem. Int. Ed. Engl.* **1968**, *7*, 565–570.
14. Hrovat, D.A.; Borden, W.T. CASSCF Calculations Find that a D_{8h} Geometry is the Transition State for Double Bond Shifting in Cyclooctatetraene. *J. Am. Chem. Soc.* **1992**, *114*, 5879–5881.
15. Borden, W.T.; Davidson, E.R. Effects of electron repulsion in conjugated hydrocarbon diradicals. *J. Am. Chem. Soc.* **1977**, *99*, 4587–4594.
16. Borden, W.T.; Iwamura, H.; Berson, J.A. Violations of Hund's Rule in Non-Kekule Hydrocarbons: Theoretical Prediction and Experimental Verification. *Acc. Chem. Res.* **1994**, *27*, 109–116.
17. Dewar, M.J.S.; Harget, A.J.; Haselbach, E. Cyclooctatetraene and Ions Derived from It. *J. Am. Chem. Soc.* **1969**, *91*, 7521–7523.
18. Ermer, O.; Klärner, F.-G.; Wette, M. Planarization of Unsaturated Rings. Cycloheptatriene with a Planar Seven-Membered Ring. *J. Am. Chem. Soc.* **1986**, *108*, 4908–4911.
19. Paquette, L. A.; Trova, M. P.; Luo, J.; Clough, A. E.; Anderson, L. B. Synthesis and Dynamic Behavior of (1,5)Cyclooctatetraenophanes. Effect of Distal Atom Bridging on Racemization Rates and Electrochemical Reducibility. *J. Am. Chem. Soc.* **1990**, *112*, 228–239.
20. Paquette, L.A.; Wang, T.-Z.; Luo, J.; Cottrell, C.E.; Clough, A.E.; Anderson, L.B. Is Pseudorotation the Operational Pathway for Bond Shifting within [8]Annulenes? Probe of Planarization Requirements by 1,3-Annulation of the Cyclooctatetraene Ring. Kinetic Analysis of Racemization and 2-D NMR Quantitation of π -Bond Alternation and Ring Inversion as a Function of Polymethylene Chain Length. *J. Am. Chem. Soc.* **1990**, *112*, 239–253.
21. Paquette, L.A. The Current View of Dynamic Change within Cyclooctatetraenes. *Acc. Chem. Res.* **1993**, *26*, 57–62.
22. Anet, F.A.L.; Bourn, A.J.R.; Lin, Y.S. Ring Inversion and Bond Shift in Cyclooctatetraene Derivatives. *J. Am. Chem. Soc.* **1964**, *86*, 3576–3577.
23. Oth, J.F.M. Conformational Mobility and Fast Bond Shift in the Annulenes. *Pure Appl. Chem.* **1971**, *25*, 573–622.

24. Kato, S.; Lee, H.S.; Gareyev, R.; Wenthold, P.G.; Lineberger, W.C.; DePuy, C.H.; Bierbaum, V.M. Experimental and Computational Studies of the Structures and Energetics of Cyclooctatetraene and Its Derivatives. *J. Am. Chem. Soc.* **1997**, *119*, 7863–7864.
25. Wenthold, P.G.; Hrovat, D.A.; Borden, W.T.; Lineberger, W.C. Transition-State Spectroscopy of Cyclooctatetraene. *Science* **1996**, *272*, 1456–1459.
26. Anet, F.A.L. The Rate of Bond Change in Cyclooctatetraene. *J. Am. Chem. Soc.* **1962**, *84*, 671–672.
27. Paquette, L.A. Ring Inversion and Bond Shifting Energetics in Substituted Chiral Cyclooctatetraenes. *Pure Appl. Chem.* **1982**, *54*, 987–1004.
28. Komatsu, K.; Nishinaga, T.; Aonuma, S.; Hirosawa, C.; Takeuchi, K.; Lindner, H.J.; Richter, J. Synthesis, Structure, and Reduction of the Cyclooctatetraene Tetra-annulated with Bicyclo[2.2.2]-octene Frameworks. *Tetrahedron Lett.* **1991**, *32*, 6767–6770.
29. Politzer, P.; Murray, J.S.; Seminario, J.M. Antiaromaticity in Relation to 1,3,5,7-Cyclooctatetraene Structures. *Int. J. Quantum Chem.* **1994**, *50*, 273–277.
30. Glukhovtsev, M.N.; Bach, R.D.; Laiter, S. Isodesmic and homodesmotic stabilization energies of [n]annulenes and their relevance to aromaticity and antiaromaticity: is absolute antiaromaticity possible? *J. Mol. Struct. THEOCHEM* **1997**, *417*, 123–129.
31. Geuenich, D.; Hess, K.; Köhler, F.; Herges, R. Anisotropy of the Induced Current Density (ACID), a General Method To Quantify and Visualize Electronic Delocalization. *Chem. Rev.* **2005**, *105*, 3758–3772.
32. Heine, T.; Corminboeuf, C.; Seifert, G. The Magnetic Shielding Function of Molecules and Pi-Electron Delocalization. *Chem. Rev.* **2005**, *105*, 3889–3910.
33. Poater, J.; Duran, M.; Solà, M.; Silvi, B. Theoretical Evaluation of Electron Delocalization in Aromatic Molecules by Means of Atoms in Molecules (AIM) and Electron Localization Function (ELF) Topological Approaches. *Chem. Rev.* **2005**, *105*, 3911–3947.
34. Gomes, J.A.N.F.; Mallion, R.B. Aromaticity and Ring Currents. *Chem. Rev.* **2001**, *101*, 1349–1384.
35. Dauben, H.J., Jr.; Wilson, J.D.; Laity, J.L. Diamagnetic Susceptibility Exaltation as a Criterion of Aromaticity. *J. Am. Chem. Soc.* **1968**, *90*, 811–813.
36. Dauben, H.J., Jr.; Wilson, J.D.; Laity, J.L. Diamagnetic Susceptibility Exaltation in Hydrocarbons. *J. Am. Chem. Soc.* **1969**, *91*, 1991–1998.
37. Chen, Z.; Wannere, C.S.; Corminboeuf, C.; Puchta, R.; Schleyer, P.v.R. Nucleus-Independent Chemical Shifts (NICS) as an Aromaticity Criterion. *Chem. Rev.* **2005**, *105*, 3842–3888.
38. Schleyer, P.v.R.; Maerker, C.; Dransfeld, A.; Jiao, H.; Hommes, N.J.R.v.E. Nucleus-Independent Chemical Shifts: A Simple and Efficient Aromaticity Probe. *J. Am. Chem. Soc.* **1996**, *118*, 6317–6318.
39. Keith, T.A.; Bader, R.F.W. Calculation of Magnetic Response Properties using a Continuous Set of Gauge Transformations. *Chem. Phys. Lett.* **1993**, *210*, 223–231.
40. Coriani, S.; Lazzeretti, P.; Malagoli, M.; Zanasi, R. On CHF Calculations of Second-Order Magnetic Properties using the Method of Continuous Transformation of Origin of the Current Density. *Theor. Chim. Acta* **1994**, *89*, 181–192.

41. A related review was reported in 2001. Klärner, F.-G. About the Antiaromaticity of Planar Cyclooctatetraene. *Angew. Chem. Int. Ed.* **2001**, *40*, 3977–3981; for reviews on the chemistry of cyclooctatetraene, see: Schröder, G. *Cyclooctatetraen*; Verlag Chemie: Weinheim, Germany, 1965; Weinheim Fray, G.I.; Saxton, R.G. *The Chemistry of Cyclooctatetraene and Its Derivatives*; Cambridge University Press: New York, NY, USA, 1978; Nishinaga, T. Cyclooctatetraenes. *Sci. Synth.* **2009**, *45a*, 383–406.
42. Gogonea, V.; Schleyer, P.v.R.; Schreiner, P.R. Consequences of Triplet Aromaticity in $4n\pi$ -Electron Annulenes: Calculation of Magnetic Shieldings for Open-Shell Species. *Angew. Chem. Int. Ed.* **1998**, *37*, 1945–1948.
43. Karadakov, P.B. Aromaticity and Antiaromaticity in the Low-Lying Electronic States of Cyclooctatetraene. *J. Phys. Chem. A* **2008**, *112*, 12707–12713.
44. Krygowski, T.M.; Pindelska, E.; Cyrański, M.K.; Häfelinger, G. Planarization of 1,3,5,7-Cyclooctatetraene as a Result of a Partial Rehybridization at Carbon Atoms: an MP2/6-31G* and B3LYP/6-311G** Study. *Chem. Phys. Lett.* **2002**, *359*, 158–162.
45. Ohmae, T.; Nishinaga, T.; Wu, M.; Iyoda, M. Cyclic Tetrathiophenes Planarized by Silicon and Sulfur Bridges Bearing Antiaromatic Cyclooctatetraene Core: Syntheses, Structures, and Properties. *J. Am. Chem. Soc.* **2010**, *132*, 1066–1074.
46. Baird, N.C. Quantum Organic Photochemistry. II. Resonance and Aromaticity in the Lowest $^3\pi\pi^*$ State of Cyclic Hydrocarbons. *J. Am. Chem. Soc.* **1972**, *94*, 4941–4948.
47. Aihara, J. Aromaticity-Based Theory of Pericyclic Reactions. *Bull. Chem. Soc. Jpn.* **1978**, *51*, 1788–1792.
48. Jug, K.; Malar, E.J.P. Geometry of Triplets and Dianions of Aromatic and Antiaromatic Systems. *J. Mol. Struct. (THEOCHEM)* **1987**, *153*, 221–226.
49. Stanger, A. Nucleus-Independent Chemical Shifts (NICS): Distance Dependence and Revised Criteria for Aromaticity and Antiaromaticity. *J. Org. Chem.* **2006**, *71*, 883–893.
50. Steiner, E.; Fowler, P.W. Four- and Two-Electron Rules for Diatropic and Paratropic Ring Currents in Monocyclic π -Systems. *Chem. Commun.* **2001**, 2220–2221.
51. Steiner, E.; Soncini, A.; Fowler, P.W. Full Spectral Decomposition of Ring Currents. *J. Phys. Chem. A* **2006**, *110*, 12882–12886.
52. Havenith, R.A.; Fowler, P.W.; Jenneskens, L.W. Persistence of Paratropic Ring Currents in Nonplanar, Tub-Shaped Geometries of 1,3,5,7-Cyclooctatetraene. *Org. Lett.* **2006**, *8*, 1255–1258.
53. Wong, H.N.C.; Garratt, P.J.; Sondheimer, F. Unsaturated Eight-Membered Ring Compounds. XI. Synthesis of sym-Dibenzo-1,5-cyclooctadiene-3,7-diyne and sym-Dibenzo-1,3,5-cyclooctatriene-7-yne, Presumably Planar Conjugated Eight-Membered Ring Compounds. *J. Am. Chem. Soc.* **1974**, *96*, 5604–5605.
54. Wong, H.N.C.; Sondheimer, F. Synthesis and Reactions of 5,6,11,12-Tetrahydrodibenzo[*a,e*]cyclooctene and 5,6-Didehydrodibenzo[*a,e*]cyclooctene. *Tetrahedron* **1981**, *37*, 99–109.
55. Huang, N.Z.; Sondheimer, F. The Planar Dehydro[8]annulenes. *Acc. Chem. Res.* **1982**, *15*, 96–102.

56. Destro, R.; Pilati, T.; Simonetta, M. Crystal structure of 5,6,11,12-tetrahydrodibenzo[a,e]cyclooctene (sym-dibenzo-1,5-cyclooctadiene-3,7-diyne). *J. Am. Chem. Soc.* **1975**, *97*, 658–659.
57. Matzger, A.J.; Vollhardt, K.P.C. Benzocyclynes Adhere to Hückel's Rule by the Ring Current Criterion in Experiment (¹H NMR) and Theory (NICS). *Tetrahedron Lett.* **1998**, *39*, 6791–6794.
58. Elix, J.A.; Sargent, M.V.; Sondheimer, F. Bicyclo[6.2.0]deca-1,3,5,7-tetraene. *J. Am. Chem. Soc.* **1967**, *89*, 180.
59. Elix, J.A.; Sargent, M.V.; Sondheimer, F. Unsaturated 8-Membered Ring Compounds. VIII. Photochemistry of 7,8-Dimethylene-1,3,5-cyclooctatrienes. Synthesis of Bicyclo[6.2.0]deca-1,3,5,7-tetraene. *J. Am. Chem. Soc.* **1970**, *92*, 969–973.
60. Pirrung, M.C.; Krishnamurthy, N.; Nunn, D. S.; McPhail, A. T. Synthesis, Structure, and Properties of a 2-(Trimethylsilyl)cyclobutenocyclooctatetraene. *J. Am. Chem. Soc.* **1991**, *113*, 4910–4917.
61. Paquette, L.A.; Wang, T.Z.; Cottrell, C.E. Flattening of the Cyclooctatetraene Ring by Annulation. *J. Am. Chem. Soc.* **1987**, *109*, 3730–3734.
62. Oda, M.; Oikawa, H. The Synthesis of Bicyclo[6.2.0]decapentaene. *Tetrahedron Lett.* **1980**, *21*, 107–110.
63. Kabuto, C.; Oda, M. Crystal and Molecular Structure of 9,10-Diphenylbicyclo[6.2.0]decapentaene a 10 π Aromatic Compound. *Tetrahedron Lett.* **1980**, *21*, 103–106.
64. Havenith, R.W.A.; Lugli, F.; Fowler, P.W.; Steiner, E. Ring Current Patterns in Annelated Bicyclic Polyenes. *J. Phys. Chem. A* **2002**, *106*, 5703–5708.
65. Kieseewetter, M.K.; Reiter, R.C.; Stevenson, C.D. The Second Cyclopropanulene: Cycloprop[8]annulene. *J. Am. Chem. Soc.* **2005**, *127*, 1118–1119.
66. Dürr, H.; Klauck, G.; Peters, K. von Schnering, H.G. A Novel Planar Antiaromatic Dibenzo[8]annulene. *Angew. Chem., Int. Ed. Engl.* **1983**, *22*, 332–333.
67. Ermer, O.; Klärner, F.-G.; Wette, M. Planarization of Unsaturated Rings. Cycloheptatriene with a Planar Seven-Membered Ring. *J. Am. Chem. Soc.* **1986**, *108*, 4908–4911.
68. Klärner, F.-G.; Ehrhardt, R.; Bandmann, H.; Boese, R.; Bläser, D.; Houk, K.N.; Beno, B.R. Pressure-Induced Cycloadditions of Dicyanoacetylene to Strained Arenes: The Formation of Cyclooctatetraene, 9,10-Dihydronaphthalene, and Azulene Derivatives; A Degenerate [1,5] Sigmatropic Shift - Comparison between Theory and Experiment. *Chem. Eur. J.* **1999**, *5*, 2119–2132.
69. Wilcox, C.F., Jr.; Uetrecht, J.P.; Grohman, K.K. Preparation of Cycloocta[def]biphenylene, a Novel Benzenoid Antiaromatic Hydrocarbon. *J. Am. Chem. Soc.* **1972**, *94*, 2532–2533.
70. Wilcox, C.F., Jr.; Uetrecht, J.P.; Grantham, G.D.; Grohmann, K.G. Synthesis and Properties of Cycloocta[def]biphenylene, a Stable Benzenoid Paratropic Hydrocarbon. *J. Am. Chem. Soc.* **1975**, *97*, 1914–1920.
71. Willner, I.; Rabinovitz, M. Cycloocta[def]fluorene: a Planar Cyclooctatetraene Derivative. Paratropicity of Hydrocarbon and Anion. *J. Org. Chem.* **1980**, *45*, 1628–1633.
72. Hellwinkel, D.; Reiff, G. Cyclooctatetraene Systems Flattened by Steric Constraints. *Angew. Chem., Int. Ed. Engl.* **1970**, *9*, 527–528.

73. Rathore, R.; Abdelwahed, S.H. Soluble Cycloannulated Tetroxa[8]circulane Derivatives: Synthesis, Optical and Electrochemical Properties, and Generation of Their Robust Cation-Radical Salts. *Tetrahedron Lett.* **2004**, *45*, 5267–5270.
74. Soulen, R.L.; Choi, S.K.; Park, J.D. Copper Coupling of 1-Chloro-2-iodo- and 1,2-Diiodoperfluorocycloalkenes. *J. Fluorine Chem.* **1973/74**, *3*, 141–150.
75. Einstein, F.W.B.; Willis, A.C.; Cullen, W.R.; Soulen, R.L. Perfluorotetracyclobutacyclooctatetraene; a Planar Eight-Memberedring System; X-ray Crystal Structure. *J. Chem. Soc. Chem. Commun.* **1981**, 526–528.
76. Baldrige, K.K.; Siegel, J.S. Quantum Mechanical Designs toward Planar Delocalized Cyclooctatetraene: A New Target for Synthesis. *J. Am. Chem. Soc.* **2001**, *123*, 1755–1759.
77. Shelton, G.R.; Hrovat, D.A.; Wei, H.; Borden, W.T. Why Does Perfluorination Render Bicyclo[2.2.0]hex-1(4)-ene Stable toward Dimerization? Calculations Provide the Answers. *J. Am. Chem. Soc.* **2006**, *128*, 12020–12027.
78. Fowler, P.W.; Havenith, R.W.A.; Jenneskens, L.W.; Soncini, A.; Steiner, E. Paratropic Delocalized Ring Currents in Flattened Cyclooctatetraene Systems with Bond Alternation. *Angew. Chem. Int. Ed.* **2002**, *41*, 1558–1560.
79. Britton, W.E.; Ferraris, J.P.; Soulen, R.L. Electrochemistry of Perfluorotetracyclobuta-1,3,5,7-cyclooctatetraene, a Powerful Neutral Organic Oxidant. *J. Am. Chem. Soc.* **1982**, *104*, 5322–5325.
80. Matsuura, A.; Komatsu, K. Efficient Synthesis of Benzene and Planar Cyclooctatetraene Fully Annelated with Bicyclo[2.1.1]hex-2-ene. *J. Am. Chem. Soc.* **2001**, *123*, 1768–1769.
81. Nishinaga, T.; Uto, T.; Inoue, R.; Matsuura, A.; Treitel, N.; Rabinoviz, M.; Komatsu, K. Antiaromaticity and Reactivity of a Planar Cyclooctatetraene Fully Annelated with Bicyclo[2.1.1]hexane Units. *Chem. Eur. J.* **2008**, *14*, 2067–2074.
82. Nishinaga, T.; Uto, T.; Komatsu, K. Novel Cyclooctatetraene Radical Cation Planarized by Full Annelation with Bicyclo[2.1.1]hexene Units. *Org. Lett.* **2004**, *6*, 4611–4614.
83. Nishinaga, T.; Komatsu, K.; Sugita, N.; Lindner, H.J.; Richter, J. First X-ray Structure of a Cyclooctatetraene Cation Radical: the Hexachloroantimonate of the Tetrakis(bicyclo[2.2.2]octeno)cyclooctatetraene Cation Radical. *J. Am. Chem. Soc.* **1993**, *115*, 11642–11643.
84. Nakamura, Y.; Aratani, N.; Shinokubo, H.; Takagi, A.; Kawai, T.; Matsumoto, T.; Yoon, Z.S.; Kim, D.Y.; Ahn, T.K.; Kim, D.; Muranaka, A.; Kobayashi, N.; Osuka, A. A Directly Fused Tetrameric Porphyrin Sheet and Its Anomalous Electronic Properties That Arise from the Planar Cyclooctatetraene Core. *J. Am. Chem. Soc.* **2006**, *128*, 4119–4127.
85. Nakamura, Y.; Aratani, N.; Furukawa, K.; Osuka, A. Synthesis and Characterizations of Free Base and Cu(II) Complex of a Porphyrin Sheet. *Tetrahedron* **2008**, *64*, 11433–11439.
86. Nakamura, Y.; Aratani, N.; Osuka, A. Experimental and Theoretical Investigations into the Paratropic Ring Current of a Porphyrin Sheet. *Chem. Asian. J.* **2007**, *2*, 860–866.
87. Schleyer, P. v. R.; Manoharan, M.; Wang, Z.-X.; Kiran, B.; Jiao, H.; Puchta, R.; van Eikema Hommes, N. J. R. Dissected Nucleus-Independent Chemical Shift Analysis of π -Aromaticity and Antiaromaticity. *Org. Lett.* **2001**, *3*, 2465–2468.
88. Corminboeuf, C.; Schleyer, P.v.R.; Warner, P. Are Antiaromatic Rings Stacked Face-to-Face Aromatic? *Org. Lett.* **2007**, *9*, 3263–3266.

89. Rzepa, H.S. Möbius Aromaticity and Delocalization. *Chem. Rev.* **2005**, *105*, 3697–3715.
90. Yoon, Z.S.; Osuka, A.; Kim, D. Möbius Aromaticity and Antiaromaticity in Expanded Porphyrins. *Nature Chem.* **2009**, *1*, 113–122.
91. Bean, D.E.; Fowler, P. W. Stacked-Ring Aromaticity: An Orbital Model. *Org. Lett.* **2008**, *10*, 5573–5576.
92. Aihara, J.-i. Origin of Stacked-Ring Aromaticity. *J. Phys. Chem. A* **2009**, *113*, 7945–7952.

© 2010 by the authors; licensee Molecular Diversity Preservation International, Basel, Switzerland. This article is an open-access article distributed under the terms and conditions of the Creative Commons Attribution license (<http://creativecommons.org/licenses/by/3.0/>).